Verification of Channel Reciprocity in Long-Range Turbulent FSO Links

Swaminathan Parthasarathy[a] (swaminathan.parthasarathy@dlr.de), Dirk Giggenbach[a] (dirk.giggenbach@dlr.de), Christian Fuchs (christian.fuchs@dlr.de), Ramon Mata-Calvo (ramon.matacalvo@dlr.de), Ricardo Barrios (ricardo.barrios@dlr.de)

Andreas Kirstädter[b] (andreas.kirstaedter@ikr.uni-stuttgart.de)
[a]Institute of Communications and Navigation, German Aerospace Centre (DLR), D-82234 Wessling;
[b]Institute of Communication Networks and Computer Engineering, University of Stuttgart, D-70569 Stuttgart

Abstract

High-Altitude Platforms / High-Altitude Pseudo Satellites (HAPs) will extend Internet access to currently uncovered regions. Free-Space Optical (FSO) links will interconnect HAPs over long distances through the stratosphere. Their Forward Error Correction has to be carefully adapted to the atmospheric scintillation channel. Long delay impairs the exploitation of receiver-based channel state information (CSI). Only inherent CSI provided by channel reciprocity allows in time control. Investigation results of this fading-signal correlation phenomenon over long distances however have not yet been reported. Therefore, we experimentally study this effect in a long-range (63km) monostatic bi-directional atmospheric FSO link for a wide range of parameters. Numerical phase-screen simulations of the transmission scenario confirm the results.

1 Introduction

Free Space Optical (FSO) communication is a potential wireless technology that provides high data rate, long distance and secure wireless communications. FSO channel reciprocity in the turbulent atmosphere is a concept resulting in a correlation of signal power at both ends of a bidirectional laser propagation link [1]. This principle has been the subject of recent studies based on experiments and simulations [2][3][4][5]. The exploitation of this effect would prove immensely beneficial for error control in FSO communication systems. In contrast to others [3] which imply diffraction-limited fiber-tracked intensity reciprocity with apertures smaller than the structures of the optical field (PIF power-into-fiber reciprocity), we investigate the more practical case of larger apertures collecting intensity focused onto a multimode power detector (PIB power-into-bucket reciprocity) [6].

In this paper, we investigate the performance of a long-range bidirectional FSO communication system in the longest ever measured ground-ground reciprocal FSO link distance of 62.86 km. We also validate the experimental observations through numerical simulations using PILab (Propagation and Imaging Lab), a Matlab based programming tool to simulate FSO communication scenarios [7][8]. The assessment of correlated received powers is performed for 5 cm and 2 cm aperture diameters (D_{rx}). The measurements were performed at different times of the day to observe channel reciprocity under different turbulence regimes. The applicability of reciprocity is projected to the use as inherent channel state information (CSI) in inter-HAP FSO links.

High Altitude Platforms (HAPs) also known as High-Altitude Pseudo Satellites are typically unmanned airplanes or airships with autonomous operation, for the purpose of providing data connectivity to mobile users underneath [9]. The operational altitudes of HAPs are in the lower stratosphere, allowing interconnect them to by laser communication links with distances from a few dozen kilometers to several hundred kilometers. In this FSO link scenario intensity speckles become larger than the receiver aperture sizes due to the long distances, enabling a high quality of reciprocity [1] [6]. Also the symmetric turbulence profile with highest turbulence in the middle of the link enhances the reciprocity effect [10][11][12].

The remainder of this paper is organized as follows: The experimental setup and its method are described in **Section 2**. In **Section 3**, an overview of the simulation parameters and its assumptions used to validate the experimental results is given. The results of the experiment are presented and discussed in detail in **Section 4**. Finally, **Section 5** concludes the paper.

2 Experiment Description

The measurement setup is depicted in Figure 1. The measurement was performed over a 62.86 km turbulent FSO bi-directional link between Augsburg (Bavarian town) hotel tower (terminal-A, 100m above ground) and German weather service (DWD) at Hohenpeissenberg mountain (terminal-B) in Germany. At each side identical transceivers were placed at a height above sea level of 596.51 m (h_A) and 949.59 m (h_B) as shown in Figure 1.

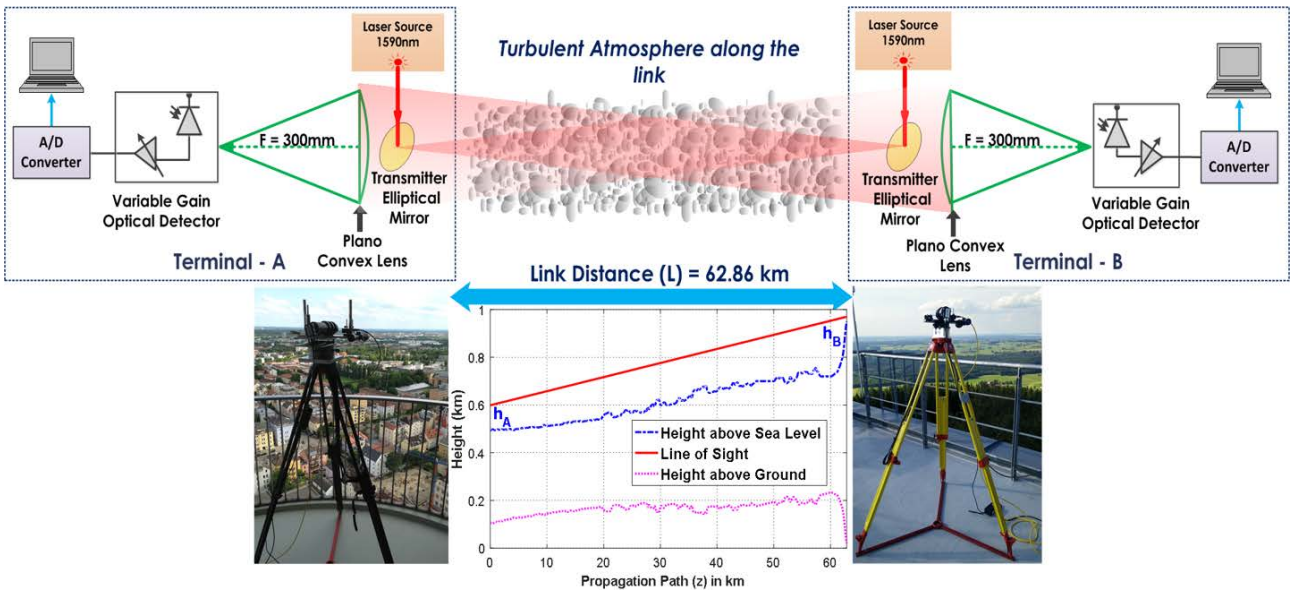

Figure 1 Measurement setup. Terminals A and B are identical optical transceivers separated by a link distance of 62.86 km. The height profile shown is along the propagation path where h_A and h_B represents the height above sea level at which the terminals A and B are placed respectively.

Totally, 16 power measurement sequences were performed between 18:30 and 22:00 (UTC+2) on July 29, 2016. The laser transmitters generated an unmodulated continuous wave Gaussian beam at a wavelength of 1590 nm with a full-angle $1/e^2$ intensity profile divergence of 506 µrad. The transmit power was varied between 2 W and 3 W. The transmit beam using a 1.27 cm protected gold coated elliptical mirror was placed in the middle of the receiver apertures of 5 cm or 2 cm. The received beam was collimated with a Plano-convex lens of F=300 mm onto a 2 mm diameter detector (resulting in 6.7mrad field of view) to a variable gain receiver connected to a 16-bit AD converter, to record the signals. 1590 nm optical filters were used to filter background light. The whole setup was mounted on a tip-tilt stage and adjusted manually to achieve maximum averaged received power signals. The received signals were simultaneously recorded at terminals A and B with sampling rate of 10 kHz for a duration of 100s each (offset + signal). The offsets (electronic and from background light) were corrected by post-processing.

3 Atmospheric Turbulence

To understand the turbulence effects on FSO link, first we need to calculate C_n^2 profile from the height above ground. The Hufnagel-Valley (HV) model [13] is the most widely used model to calculate C_n^2 profile (which scales the atmosphere's IRT structure function). This model cannot be used for our scenario as here we are in a near-ground situation (few meters to ~250 m above the ground level) that is nearly a horizontal path. For our numerical simulations, we use so called Walters and Kunkel model [14] given by

$$C_n^2(h) = C_n^2(h_0)(h_0/h)^p \qquad (1)$$

where h_0 represents a reference height above ground, and h is the height profile above ground. $C_n^2(h_0)$ is the reference refractive index structure value at h_0. The power law parameter p varies from 4/3 during the daytime to 2/3 for measurements between sunset and sunrise [14]. We assume p = 2/3 based on our measurements time and h_0 as 1 m. Three values of $C_n^2(h_0)$ were selected as $6.50e^{-16}$, $1.20e^{-15}$ and $8.11e^{-15}$ for h_0 = 1 m. The selected values were obtained as a best fit for measured scintillation index values 0.301, 0.537 and 1.309 respectively as shown in Table I. Regarding that in inter-HAP links this C_n^2 will be much smaller and vary less due to the smoother C_n^2-height profile in stratospheric altitudes [11] [12]. A transmit beam with large divergence can be approximated as spherical wave in our scenario according to p. 281 of [13]. The spherical wave Rytov variance is $\beta_0 = 0.4\sigma_R^2$, where σ_R^2 is the plane wave Rytov variance. The normalized variance of received power P into a given aperture size D_G, is the Power Scintillation Index (PSI) given by [13]:

$$\sigma_I^2(D_G) = \frac{\langle P^2 \rangle - \langle P \rangle^2}{\langle P \rangle^2} \qquad (2)$$

where $\langle . \rangle$ represents time averaging. In this work, we evaluate our measurement and numerical simulation results based on parameters such as Power Scintillation Index (PSI), Correlation Coefficient (CCF), Normalized Mean Squared Error (NMSE), and Half Width Half Max-

imum auto-covariance (HWHM acov.). CCF and NMSE are defined as follows [15][16]:

$$CCF = \frac{E\{(A_i - \mu_A)(B_i - \mu_B)\}}{\sigma_A \sigma_B} \quad (3)$$

$$NMSE = \frac{\sum_{i=1}^{N} (A_i - B_i)^2}{\mu_A \mu_B} \quad (4)$$

where A_i and B_i are received optical powers over time measured at terminals A and B, and μ and σ represent their means and standard deviations respectively. $E\{\}$ is the expected value operator. Both CCF and NMSE are used together here as metric to evaluate the quality of reciprocity. The reason is being that CCF does not regard the absolute power variations of the received power vector. Whereas NMSE results in error differences of the absolute power variations. The value of CCFs below 1 or NMSE above 0 respectively represent the (real-world) imperfectness of this channel state information.

4 Results and Discussion

In this section, we present the experimental results and a detailed analysis of the results. In addition, we also confirm the results using numerical phase-screen simulations.

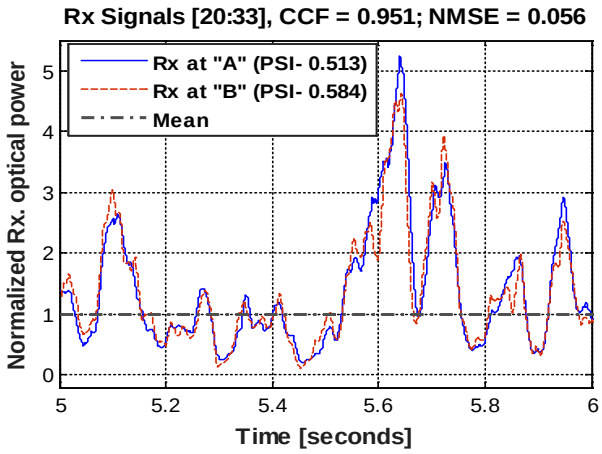

Figure 2 Simultaneously measured received optical powers at terminals A and B for 5cm D_{rx} for measurement sequence [20:33] as shown in Table 1.

Figure 2 depicts typical measured optical powers at both terminals and Figure 3 shows the observed variations of CCF, NMSE and PSI over measurement time. Table I shows the summary of measurement results with different parameters. The measurements were performed starting before sunset until night time resulting in CCFs from 0.984 (2 cm D_{rx}) to 0.803 (5 cm D_{rx}), PSIs from 0.24 to 2.1, HWHM acov. from 11.05 ms to 43.65 ms. From Table1, we observe that the mean received power at terminal-B is always lower than at terminal-A, due to higher beam spread near A (more turbulent link end). The loss due to inner obscuration of the transmit mirror is regarded in calculations of mean power that is ~63% and 25% for 2 cm and 5 cm D_{rx} respectively. PSIs at B are always higher than at A which we expect due to higher turbulence near terminal A as seen from C_n^2 -profiles in Figure 6 (non-symmetric C_n^2 profile).

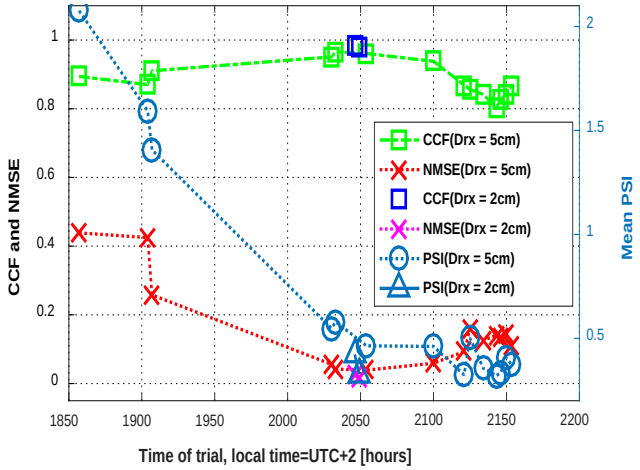

Figure 3 Overall observed CCF, NMSE and mean PSI variations over measurement time.

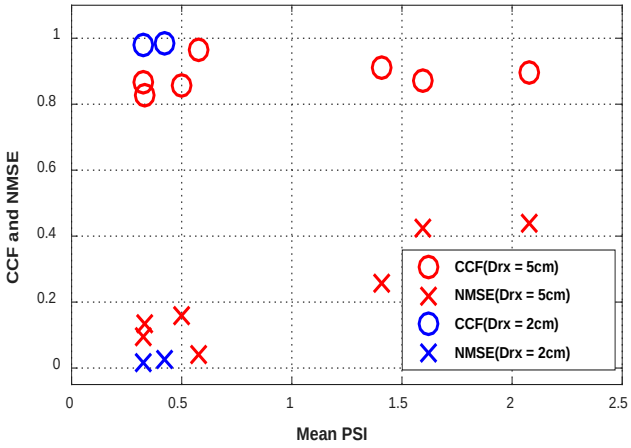

Figure 4 CCF and NMSE for different mean PSI.

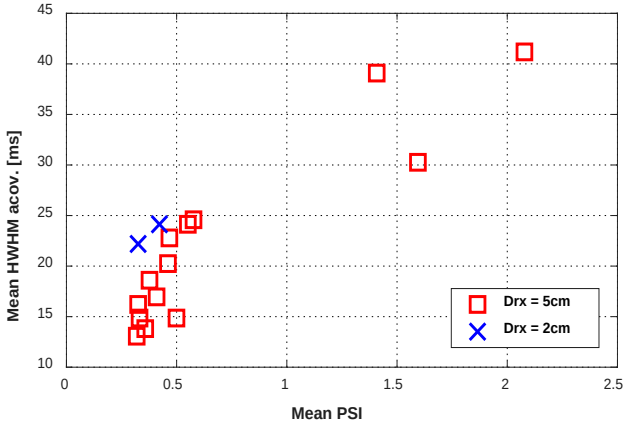

Figure 5 Mean HWHM acov. versus mean PSI. Mean refers to average of parameters at A and B.

Time of Measurement sequence (German local time)[a]	Mean received power at A (nW)	Mean received power at B (nW)	PSI at A	PSI at B	HWHM acov. at A (ms)	HWHM acov. at B (ms)	CCF	NMSE
18:57	368.64	226.92	2.034	2.118	43.65	38.65	0.894	0.4385
19:04	375.73	185.18	1.4509	1.739	32.35	28.05	0.8702	0.425
19:07	405.78	201.63	1.309	1.504	40.75	37.45	0.9104	0.258
20:30	277.13	227.94	0.513	0.584	25.05	23.35	0.9509	0.056
20:33	272.91	237.11	0.537	0.622	25.45	23.75	0.966	0.042
20:46[b]	20.29	18.54	0.352	0.493	24.15	24.05	0.984	0.025
20:49[b]	21.57	20.80	0.301	0.353	22.35	21.95	0.9807	0.014
20:54	366.86	317.69	0.430	0.498	23.65	22.05	0.9608	0.039
21:00	371.05	300.57	0.425	0.497	21.55	19.05	0.938	0.059
21:21	386.68	264.41	0.271	0.377	18.15	14.15	0.869	0.093
21:25	402.6	241.02	0.411	0.593	16.75	13.05	0.856	0.159
21:34	401.85	682.85	0.283	0.431	15.75	11.95	0.842	0.125
21:43	697.48	638.41	0.243	0.397	15.15	11.05	0.803	0.141
21:46	690.84	615.41	0.255	0.414	16.75	12.85	0.826	0.132
21:50	720.39	612.98	0.317	0.495	18.65	15.15	0.844	0.143
21:53	700.42	579.68	0.308	0.446	20.55	16.65	0.866	0.112

Table 1 Summary of measurement results for 62.86 km bi-directional FSO link. [a]All measurements were performed on July 29, 2016; local time = UTC+2; sun set: 21:30 local time, [b]For receiver aperture diameter D_{rx}= 2 cm

Figure 4 shows the changes in CCF values for different mean PSI values for D_{rx} 2 cm and 5 cm. We see that high CCFs are observed not only for PSIs < 1 but also in strong turbulence for PSIs > 1, proving that high correlation can be achieved even at strong turbulence conditions. Also, we see that for PSIs > 1, NMSEs are higher.

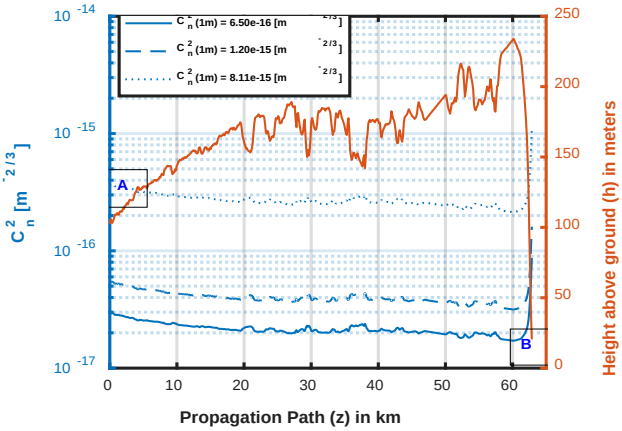

Figure 6 C_n^2-profile along the propagation path z (terminal A on Augsburg-Tower, terminal B at DWD-Hohenpeissenberg). The path height refers to height above the ground and 3 different C_n^2-profiles used for PILab simulations are shown for chosen C_n^2-profile at 1m (h_0).

Figure 5 shows mean HWHM acov. for different mean scintillation strengths. We observed faster scintillations during weaker turbulences (with PSIs < 0.5), and slower (almost twice the auto covariance time) for PSIs > 1. This effect is due to the change in wind speed acting orthogonally to the link. Also, in general the channel got slower and scintillation strength decreased towards sunset and at night as seen in Table 1.

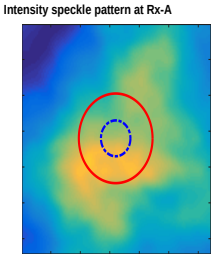

Figure 7 PILab simulated intensity speckle patterns at receivers A and B. The circles represent two different D_{rx} 2cm and 5cm. The x and y axis are in pixels with each pixel = 1mm. The color bars represent absolute intensity values equally scaled.

To reproduce the measured behavior by PILab simulations, we selected three different measured vectors corresponding to three different scintillation strengths and CCFs with two 5 cm and one 2 cm D_{rx}. The representing PSI values range from ~0.3 to 1.5 which represents weak to strong turbulent conditions [13]. The C_n^2 profile calculated using (1) was used assuming different turbulent conditions by varying $C_n^2(h_0)$ at h_0 = 1 m as shown in Figure 6. PILAB uses atmospheric propagation simulations in which the spatial and temporal dynamic of the atmospheric turbulence is modelled by phase screens that are shifted laterally according to the orthogonal wind. The temporal fluctuations of the received power signals are induced due to these orthogonal winds which were assumed 1 m/s to 2 m/s (corresponds to measured HWHM acov.).

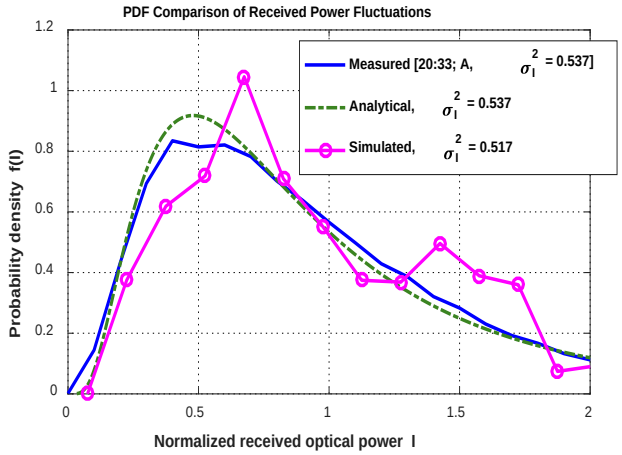

Figure 8 Comparison of the obtained received power fluctuations PDFs obtained from measurement, PILab simulation and analytical distribution for D_{rx} 5cm.

Figure 7 depicts an example of two instantaneous received intensity fields simulated with PILab. Figure 8 shows an example of the comparison of PDF estimate calculated using lognormal distribution compared with measurement and simulation. We see that the results match well with the analytical and simulated for PSI 0.537 (measured). The outliers of the simulated values PDF is due to the limited continuous vector length as given by the finite size of phase screens moved with the lateral wind speed.

Parameters	EXP [19:07]	SIM	EXP [20:33]	SIM	EXP[a] [20:49]	SIM[a]
PSI-A	1.309	1.359	0.537	0.517	0.301	0.337
PSI-B	1.504	1.167	0.622	0.561	0.353	0.361
CCF	0.91	0.93	0.96	0.91	0.98	0.92
NMSE	0.258	0.178	0.042	0.09	0.014	0.055
HWHM acov. -A (ms)	40.75	35.65	25.45	23.95	22.35	29.75
HWHM acov. -B (ms)	37.45	32.65	23.75	24.35	21.95	26.65

Table 2 Comparison of experimental observations and PILab simulations, [a]For receiver aperture diameter D_{rx}= 2 cm

As shown in Table 2, our measured and simulated results agree well, based on several parameters. We performed an averaging of five (very time consuming) time series for this PDF, resulting in a total power vector length of 10s.

5 Conclusions and Outlook

In this paper, we investigated the performance of long-range bidirectional FSO communication and for the first time proved the existence of reciprocity over a longest ever measured ground-ground bidirectional FSO link. Our experimental evidence and numerical simulations confirms the existence of strong correlations.

This inherent and lowest delay CSI then offers promising opportunities to overcome the effects of signal scintillation guaranteed by turbulence in atmospheric FSO links: The gained high-quality and real-time knowledge about the current channel conditions so called “Reciprocal CSI” can be exploited in adaptive transmission techniques such as adaptive code- or data-rate, and hybrid ARQ techniques. The reciprocal CSI also reduces the retransmission time by half in multi-hop HAP systems compared to conventional ARQ protocols. This promises to be advantageous for multi-hop FSO links, as they are intended for future HAP-based global communication networks.

6 Literature

[1] J. H. Shapiro, “Reciprocity of the turbulent atmosphere,” *J. Opt.Soc. Am.*, vol. 61, no. 4, pp. 492–495, Apr. 1971.

[2] D. Giggenbach, W. Cowley, K. Grant, and N. Perlot, “Experimental verification of the limits of optical channel intensity reciprocity,” *Appl. Opt.*, vol. 51, pp. 3145-3152, 2012.

[3] R. R. Parenti, J. M. Roth, J. H. Shapiro, F. G. Walther, and J. A. Greco, “Experimental observations of channel reciprocity in single-mode free-space optical links,” Opt. Express 20, pp. 21635-21644, 2012.

[4] J. Minet, M. A. Vorontsov, E. Polnau, and D. Dolfi, “Enhanced correlation of received power-signal fluctuations in bidirectional optical links,” *Journal of Optics.*, vol. 15 Issue 2, pp. 022401, 2013.

[5] Z. Kolka, V. Biolkova, O. Wilfert and D. Biolek, "Simulation model of correlated FSO channels," 2015 Conference on Microwave Techniques (COMITE), Pardubice, pp. 1-4, 2015.

[6] S. Parthasarathy, D. Giggenbach, R. Barrios, C. Fuchs, A. Kirstädter, “Simulative Verification of Channel Reciprocity in Free-Space Optical Inter-HAP Links,” International Conference on Space Optical Systems (ICSOS), pp. 14-16, 2017.

[7] J. Horwath, N. Perlot, D. Giggenbach, R. Jüngling, “Numerical simulations of beam propagation through optical turbulence for high-altitude platform crosslinks,” *Proc. SPIE*, vol. 5338, Free-Space Laser Communication Technologies XVI, pp. 243, June. 16, 2004

[8] N. Perlot, J. Horwath, R. Jüngling, “Modeling wind in simulations of atmospheric optical propagation,” *Proc. SPIE*, vol. 5712, Free-Space Laser Communication Technologies XVII, pp. 140, May 02, 2005

[9] T. C. Tozer and D. Grace, “High-altitude platforms for wireless communications,” *Electronics & Communication Engineering Journal*, vol. 13, no. 3, pp. 127-137, June 2001.

[10] D. Giggenbach, R. Purvinskis, M. Werner, M. Holzbock, “Stratospheric Optical Inter-Platform Links for High Altitude Platforms,” Online Proceedings. 20th AIAA International Communications Satellite Systems Conference, 2002.

[11] S. Parthasarathy, A. Kirstaedter and D. Giggenbach, “Performance Analysis of Adaptive Hybrid ARQ for Inter-HAP Free-Space Optical Fading Channel with Delayed Channel State Information,” Photonic Networks; 17. ITG-Symposium; Proceedings of, Leipzig, Germany, pp. 1-7, 2016.

[12] S. Parthasarathy, A. Kirstaedter and D. Giggenbach, “Adaptive HARQ with Channel State Information in Inter-HAP FSO Links,” Photonic Networks; 18. ITG-Symposium, Leipzig, Germany, 2017, pp. 1-6.

[13] L. C. Andrews and R. C. Phillips, “Laser Beam Propagation through Random Media - Second Edition,” SPIE-Press, Bellingham, 2005.

[14] F. G. Smith (Ed.), “Atmospheric Propagation of Radiation, The Infrared & Electro-Optical Systems Handbook (3rd Edition),” vol. 2 , SPIE Optical Engineering Press, 1993.

[15] Z. Wang and A. C. Bovik, “Mean squared error: Love it or leave it? A new look at Signal Fidelity Measures,” *IEEE Signal Processing Magazine*, vol. 26, no. 1, pp. 98-117, Jan. 2009.

[16] L. Mandel, E. Wolf, “Optical Coherence and Quantum Optics,” Cambridge: Cambridge University Press., 1995.